PERGAMON

International Journal of Heat and Mass Transfer 45 (2002) 357–366

International Journal of HEAT and MASS TRANSFER

www.elsevier.com/locate/ijhmt

A model of through-air drying of tufted textile materials

H. Stephen Lee, Wallace W. Carr *, Haskell W. Beckham, Johannes Leisen

School of Textile and Fiber Engineering, Georgia Institute of Technology, Atlanta, GA 30332, USA

Received 30 June 2000; received in revised form 2 April 2001

Abstract

A transient two-dimensional mathematical model is developed to simulate the through-air drying process for tufted textile materials. The heat and mass transfer in a cylindrical porous medium and the air flowing around it are analyzed separately. First, thermal and mass circuits are used to analyze the simultaneous heat and mass transfer within the porous medium. Then, the equations of the conservation of mass and energy are written for the drying medium. The resulting system of three non-linear differential equations is numerically solved by an implicit finite difference method. The numerical solutions are compared with experimental drying results obtained using magnetic resonance imaging (MRI) and a laboratory through-air dryer (LTAD). © 2001 Elsevier Science Ltd. All rights reserved.

1. Introduction

Drying is a time-consuming, energy intensive and expensive process required after most dyeing and/or finishing processes in the textile industry. The focus of this investigation was the development of a mathematical model to simulate the through-air drying process of tufted textile materials (carpet), which accounts for more than 90% of the carpet produced in the US [1]. Brock and Gorton [2] showed that through-air drying can be applied to the unbacked tufted carpet and that through-air drying time is approximately one-fifth of the time required in cross-flow industrial dryers. Through-air drying is more effective because airflow through the carpet increases the contact between individual yarns and the hot air. Thus, the through-air dryer is the most commonly used equipment for drying unbacked, dyed tufted carpet. An accurate mathematical model is needed to assist carpet manufacturers in controlling and/or optimizing their current operations, increasing production rate and decreasing energy cost.

Many theoretical models [3–21] have been proposed for convectively drying hundreds of moist porous materials in the agricultural, ceramic, food, pharmaceutical, pulp and paper, mineral, polymer and textile industries. Waananen et al. [22] discuss many of these drying models, including structural and thermodynamic assumptions, controlling process resistance, internal mechanisms of moisture movement, model solutions, and experimental approaches to validate the models. In general, a moist porous solid is entirely composed of a wet region before drying commences. The wet region contains unbound (free) moisture, and capillary flow dominates the liquid moisture transport in this region. A sorption region appears when the moisture regain (moisture content on dry basis) falls below the maximum sorptive value. A moving front divides the porous medium into the sorption region and the wet region. In the sorption region which contains no unbound moisture, the liquid-phase moisture transport is dominated by bound moisture flow, and the gas-phase moisture transport is dominated by water vapor diffusion. The front will recede until the wet region disappears; i.e., the entire porous solid consists of the sorption region. There are several models [4–6,8,11,12] of simultaneous heat, mass and momentum transfer in the two regions of the porous solids. These models are based on the equations of conservation of energy, conservation of mass and conservation of momentum together with the necessary physical and transport properties.

A transient two-dimensional mathematical model, which considered primary heat, moisture and momentum transfer mechanisms in the moist porous material

* Corresponding author. Tel.: +1-404-894-2538; fax: +1-404-894-8780.

E-mail address: wallace.carr@tfe.gatech.edu (W.W. Carr).

0017-9310/02/$ - see front matter © 2001 Elsevier Science Ltd. All rights reserved.
PII: S0017-9310(01)00130-2

Nomenclature

c_p	specific heat (J/kg K)
D_{eff}	effective binary diffusion coefficient (m^2/s)
h_{fg}	latent heat of vaporization for water (J/kg)
h_m	convective mass transfer coefficient (m/s)
h_T	convective heat transfer coefficient (W/m^2 K)
j	mass flux (kg/s)
k_{eff}	effective thermal conductivity (W/m K)
L	carpet thickness (mm)
Le	dimensionless Lewis number
m	mass (kg)
$\dot{m}$	evaporation rate (kg/s)
m_y	yarn mass (kg)
P_{atm}	atmospheric pressure (N/m^2)
q	heat transfer rate (W)
r	radial direction
r_f	position of evaporation front (mm)
r_M	mean radius (mm)
R	yarn diameter (mm)
$\overline{R}$	universal gas constant
Rm	mass resistance (s/m^3)
Rt	thermal resistance, m^2 K/W
t	time
T	temperature (K)
T_M	mean temperature (K)
V	apparent velocity (m/min)
X	moisture regain
Y	humidity ratio of moist air
z	z direction; pile yarn direction

Greek symbols

ε_c	inter-yarn porosity
ε_y	intra-yarn porosity
ρ	density (kg/m^3)
τ	correction factor

Subscripts

0	initial
1	region between air stream and yarn surface
2	region between yarn surface and evaporation front; region between yarn surface and mean position of the dry region
3	region between yarn mean position of the dry region and wet region surface
a	dry air
a^∞	air in the air flow
crit	critical
room	room condition
s	solid phase
surf	yarn surface
tot	total
v	water vapor
va^∞	water vapor in the air flow
vs	saturated water vapor
w	water
wet	wet region in the yarn

(yarn) and drying medium (airflow), was developed for through-air drying of tufted carpet [12]. The drying model consisted of two sets of coupled differential equations with relevant initial and boundary conditions. The model contained a number of unknown physical and transport properties. With the number of unknown physical and transport properties, the model is not very useful for industrial applications. Thus, a simpler model requiring fewer physical and transport properties, but capable of accurately predicting temporal one-dimensional moisture profiles, and thus overall moisture regain and drying time, was developed. The simplified drying model is presented here.

A difficulty often encountered in evaluating the accuracy of drying models is the lack of experimental data on the moisture profiles in anisotropic porous media. However, research [23–25] at Georgia Institute of Technology has shown that moisture distributions within porous media can be accurately monitored during drying using a magnetic resonance imaging (MRI) technique. In the present study, MRI was used to continuously record one-dimensional moisture profiles during drying. In addition to MRI, a laboratory through-air dryer (LTAD), which closely simulates the industrial process [12,26], was used to obtain variations of overall moisture regain with time at industrial drying conditions. Numerical predictions from the model were compared with experimental drying data from both systems.

2. Theoretical drying model

The porous medium studied was unbacked cut-pile nylon carpet. Unbacked tufted carpet consists primarily of short lengths of yarn, typically 5–20 mm long. These yarns, referred to as face yarn, are held in position by a very thin woven fabric, called primary backing. The face yarns are packed nearly parallel to each other and run perpendicular to the primary backing. Since the primary backing is typically made of polypropylene and holds little moisture, it is neglected in our model. Fig. 1 shows schematically the top view of the arrangement of yarns. The holes through which pairs of yarns penetrate the primary backing can be seen. Not shown are small sections of yarn, located on the backside of the primary backing and extending between the yarns in the rows of holes. Since the length of the yarn on the backside is

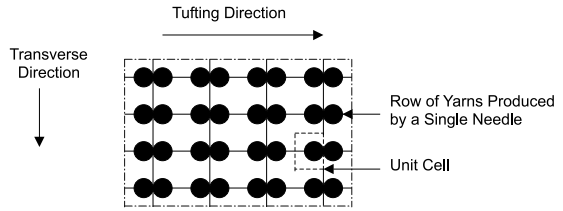

Fig. 1. Schematic of the top view of the structure of the carpet and the unit cell.

small compared to the length of the face yarn, we simplify the geometry by adding the length of the yarn on the backside to the length of face yarn. The unit cell (see Fig. 2) is a yarn and the surrounding space through which air flows parallel to the yarn. The yarn is considered to be a porous circular cylinder.

In Fig. 3, two-dimensional magnetic resonance (MR) images of moisture in a slice of a single carpet yarn are shown as a function of drying time. The imaging plane is perpendicular to the yarn axis. The images clearly reveal the moisture front between the wet and sorption regions recedes from the outer region of the reference circle to the inner region during drying. Thus, moisture transport varies in the radial direction. Coupled with the varying airflow temperature and humidity ratio in the airflow direction (i.e., parallel to the yarn axis), this indicates a transient two-dimensional drying model is needed to describe mass and heat transfer during the through-air drying process [12]. The model has two parts: the first is a model for heat and mass transfer in the yarn, and the second is a model for heat and mass transfer in airflow. It is assumed that the airflow is along the surface of the yarn, but does not penetrate into the yarn.

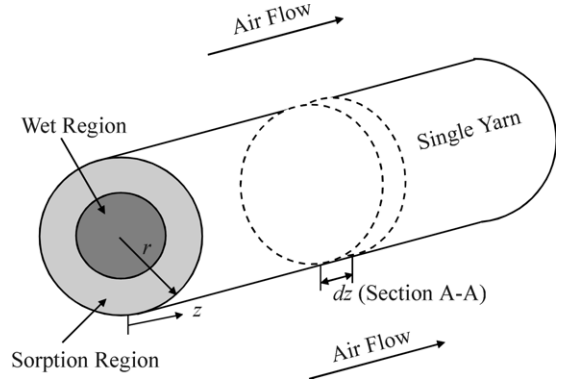

Fig. 2. Schematic of a yarn and its immediate surrounding space inside the unit cell.

2.1. Model for heat and mass transfer in the yarn

The yarn model is developed by considering mass and heat transfer within the wet and sorption regions of the differential control volume in a given slice of yarn (see Section A-A in Fig 2). Heat and moisture transport are assumed to vary only in the radial direction. First, consider moisture and momentum transport within the wet region. Capillary flow dominates the unbound moisture flow in this region. It is assumed that capillary flow maintains a uniform moisture distribution in the wet region for moisture regain greater than the critical moisture regain. When critical moisture regain is reached in a given slice of yarn, the evaporation front begins to recede from the yarn surface, and the moisture regain in the wet region is maintained at the critical value. In the sorption region, moisture regain is assumed to be 0. Thus, the region is referred to as the dry region, and bound moisture transport within this region is neglected. The rate of change in mass of stored water vapor is ignored in the dry region. Evaporating water at the front diffuses through the dry region to the yarn surface. Then, the water vapor at the surface is convectively transferred into the airflow.

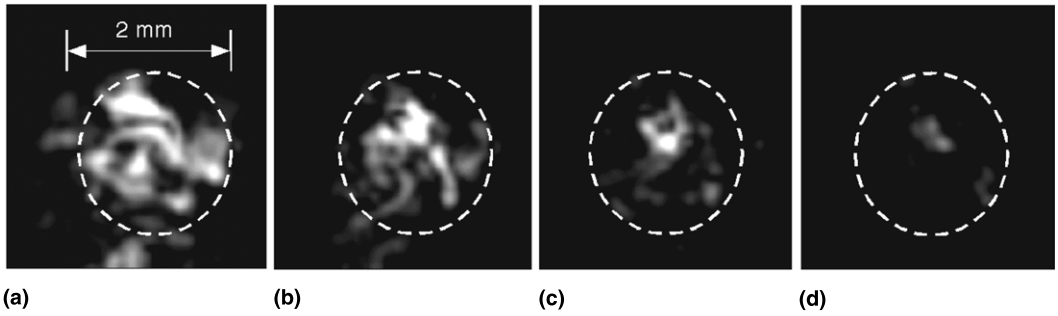

Fig. 3. Two-dimensional MR images of moisture in a slice of a single carpet yarn as a function of drying time at 25°C using an airflow of 3 L/min. The imaging plane is perpendicular to the yarn axis. Lighter areas represent higher moisture content. The moisture front recedes radially inward during drying. (a) 0–15, (b) 120–135, (c) 240–255 and (d) 360–375 s.

Consider the heat transfer from the air stream to the yarn. The heat transfer rate from the air stream to the yarn surface, q_{tot}, is equal to rate of the energy stored in the dry region, q_{sorp}, plus rate of the energy transferred to the wet region, q_{wet}. In the dry region, transient, one-dimensional (r direction, see Fig. 2) heat conduction is assumed. The energy stored in the dry region is treated as though it is all located at the mean radius, r_{M}, which divides the dry area in half; i.e., half of the dry area is from r_{f} to r_{M}, and half of the dry area is from r_{M} to R (see Fig. 4). The energy transferred to the wet region by heat conduction evaporates water and/or increases stored energy. The temperature distribution is assumed to be uniform in the wet region.

In this study, the thermal and mass transfer circuits, shown in Fig. 4, are used to write the energy and mass balance equations in the model. The resistance to mass transfer from the air stream to the yarn surface is Rm_1. The resistance to mass transfer from the yarn surface to the evaporation front is Rm_2. The resistance to heat transfer from the air stream to the yarn surface is Rt_1. The thermal resistance through the dry region is divided into two parts based on a mean radius, r_{M}, as mentioned above. The mean radius, r_{M}, may be written as

$$r_{\text{M}} = \sqrt{\frac{R^2 + r_{\text{f}}^2}{2}}. \tag{1}$$

The resistance to heat transfer from the yarn surface to the mean position of the dry region is Rt_2. The resistance to heat transfer from the mean position of the dry region to the surface of the wet region is Rt_3.

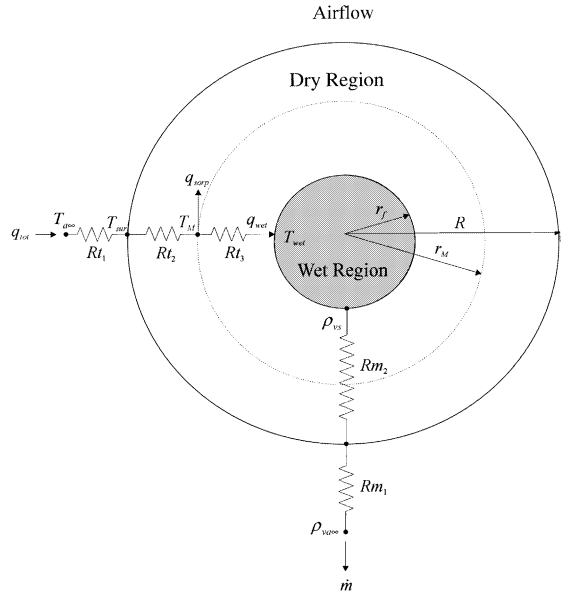

Fig. 4. Thermal and mass circuits for the yarn and airflow in Section A–A (see Fig. 2).

Mass transfer from the evaporation front to the air steam can be modeled as a series circuit as shown in Fig. 4. Thus, the evaporation rate, $\dot{m}$, can be written as

$$\dot{m} = \frac{\lfloor \rho_{\text{vs}}(r = r_{\text{f}}, z, t) - \rho_{va\infty} \rfloor}{Rm_{\text{tot}}}, \tag{2}$$

where ρ_{vs} and $\rho_{va\infty}$ are the densities of the saturated water vapor at the evaporation front and the water vapor in the airflow, respectively, and the total mass resistance, Rm_{tot}, is

$$Rm_{\text{tot}} = Rm_1 + Rm_2 = \frac{1}{h_m 2\pi R\,\mathrm{d}z} + \frac{\ln(R/r_{\text{f}})}{2\pi D_{\text{eff}}\,\mathrm{d}z}, \tag{3}$$

where D_{eff} is the effective diffusivity and h_m is the convective mass transfer coefficient.

The total energy transferred to the yarn, q_{tot}, is

$$q_{\text{tot}} = \dot{m}h_{fg} + \left[\left(\frac{r_{\text{f}}^2}{R^2}\right)m_{\text{s}}c_{\text{ps}} + m_{\text{w}}c_{\text{pw}}\right]\frac{\partial T_{\text{wet}}}{\partial t} + \left(1 - \frac{r_{\text{f}}^2}{R^2}\right)m_{\text{s}}c_{\text{ps}}\frac{\partial T_{\text{M}}}{\partial t}, \tag{4}$$

where h_{fg} is the latent heat of vaporization of water, m_{s} is the mass of fibers, m_{w} is the mass of liquid water, and r_{f} is the position of the evaporation front. The position of the evaporation front is defined as

$$r_{\text{f}} = \begin{cases} R & \text{if } X(z,t) \geqslant X_{\text{crit}}, \\ \sqrt{\frac{X(z,t)}{X_{\text{crit}}}}R & \text{if } X(z,t) < X_{\text{crit}}, \end{cases} \tag{5}$$

where X_{crit} is the critical moisture regain. The mean temperature of the dry region,T_{M}, is

$$T_{\text{M}} = T_{\text{wet}} + \frac{\ln(r_{\text{M}}/r_{\text{f}})}{2\pi k_{\text{eff}}\,\mathrm{d}z}q_{\text{wet}}, \tag{6}$$

where k_{eff} is the effective thermal conductivity.

Additionally, the total energy transferred to the yarn may be expressed as

$$q_{\text{tot}} = \frac{T_{a\infty} - T_{\text{M}}}{Rt_1 + Rt_2}, \tag{7}$$

where Rt_1 and Rt_2 are defined as

$$Rt_1 = \frac{1}{2\pi R h_T\,\mathrm{d}z}, \quad Rt_2 = \frac{\ln(R/r_{\text{M}})}{2\pi k_{\text{eff}}\,\mathrm{d}z},$$

where h_T is the convective heat transfer coefficient.

Therefore, the equation of energy conservation may be expressed as

$$\frac{T_{a\infty} - T_{\text{M}}}{Rt_1 + Rt_2} = \dot{m}h_{fg} + \left[\left(\frac{r_{\text{f}}^2}{R^2}\right)m_{\text{s}}c_{\text{ps}} + m_{\text{w}}c_{\text{pw}}\right]\frac{\partial T_{\text{wet}}}{\partial t} + \left(1 - \frac{r_{\text{f}}^2}{R^2}\right)m_{\text{s}}c_{\text{ps}}\frac{\partial T_{\text{M}}}{\partial t}. \tag{8}$$

Since the air and water vapor are assumed to be ideal gases, $\rho_{\text{vs}}(r = r_{\text{f}}, z, t)$ and $\rho_{va\infty}$ may be found [27]

$$\rho_{vs}(r=r_f,z,t)=\frac{P_{vs}}{\bar{R}T_{wet}}, \tag{9}$$

$$\rho_{va^\infty}=\frac{YP_{atm}}{(0.622+Y)\bar{R}T_{a^\infty}}, \tag{10}$$

where Y is the humidity ratio, and T_{a^∞} is the air temperature.

Substituting Eqs. (9) and (10) into Eq. (8) gives

$$\begin{aligned}\frac{T_{a^\infty}-T_M}{Rt_1+Rt_2}=&\left\{\left(\left[\frac{P_{vs}}{\bar{R}T_{wet}}-\frac{YP_{atm}}{(0.622+Y)\bar{R}T_{a^\infty}}\right]h_{fg}\right)\Big/Rm_{tot}\right\}\\&+\left[\left(\frac{r_f^2}{R^2}\right)m_sc_{ps}+m_wc_{pw}\right]\frac{\partial T_{wet}}{\partial t}\\&+\left(1-\frac{r_f^2}{R^2}\right)m_sc_{ps}\frac{\partial T_M}{\partial t}.\end{aligned} \tag{11}$$

2.2. Model for heat and mass transfer in the airflow

Consider conservation of heat and mass transfer in the differential control volume of the airflow. Heat and mass balance equations may be written as

$$\left(\rho_{a^\infty}\frac{\partial Y}{\partial t}+j_{a^\infty}\frac{\partial Y}{\partial z}\right)dz=\dot{m}, \tag{12}$$

$$(c_{pa}+Yc_{pv})\left(\rho_{a^\infty}\frac{\partial T_{a^\infty}}{\partial t}+j_{a^\infty}\frac{\partial T_{a^\infty}}{\partial z}\right)dz=q_{tot}. \tag{13}$$

Initial and boundary conditions for each dependent variable (Y and T_{a^∞}) are required to solve the set of the governing equations. Initial conditions for humidity ratio and air temperature are assumed to be constant and are

$$Y(z,t=0)=Y_0, \tag{14}$$

$$T_{a^\infty}(z,t=0)=T_{a^\infty,room}. \tag{15}$$

At the entrance of the airflow ($z=0$), humidity ratio and air temperature are assumed to be constant during drying and are given as

$$Y(z=0,t)=Y_0, \tag{16}$$

$$T_{a^\infty}(z=0,t)=T_{a^\infty 0}. \tag{17}$$

3. Numerical analysis

Using the implicit finite difference approximation, the discretized form at the time step $(j+1)$ for Eq. (11) may be expressed as

$$\begin{aligned}F(T_{wet,m}^{j+1})=&\frac{T_{a^\infty,m}^{j}-T_{M,m}^{j+1}}{Rt_{1,m}^{j}+Rt_{2,m}^{j}}\\&-\left\{\left(\left[\frac{P_{vs,m}^{j+1}}{\bar{R}T_{wet,m}^{j+1}}-\frac{Y_m^jP_{atm}}{(0.622+Y_m^j)\bar{R}T_{a^\infty,m}^{j}}\right]h_{fg,m}^{j}\right)\Big/Rm_{tot,m}^{j}\right\}\\&-\left[\left(\frac{r_{f,m}^{j}}{R}\right)^2m_sc_{ps}+m_{w,m}^{j}c_{pw}\right]\frac{T_{wet,m}^{j+1}-T_{wet,m}^{j}}{\Delta t}\\&-\left[1-\left(\frac{r_{f,m}^{j}}{R}\right)^2\right]m_sc_{ps}\frac{T_{M,m}^{j+1}-T_{M,m}^{j}}{\Delta t}=0.\end{aligned} \tag{18}$$

Since $T_{wet,m}^{j+1}$ is the only independent variable in the above equation, a numerical method to find a root of $F(T_{wet,m}^{j+1})=0$ is necessary. In this study, the bisection method [28] is used to obtain the root of $F(T_{wet,m}^{j+1})=0$, that is accurate within a specified tolerance value.

Once $T_{wet,m}^{j+1}$ is found, the evaporation rate, $\dot{m}_m^{j+1}$, and the mass of liquid water, $m_{w,m}^{j+1}$, are determined using the following expressions:

$$\dot{m}_m^{j+1}=\left[\frac{P_{vs,m}^{j+1}}{\bar{R}T_{wet,m}^{j+1}}-\frac{Y_m^jP_{atm}}{(0.622+Y_m^j)\bar{R}T_{a^\infty,m}^{j}}\right]\Big/Rm_{tot,m}^{j}, \tag{19}$$

$$m_{w,m}^{j+1}=m_{w,m}^{j}-\dot{m}_m^{j+1}\Delta t. \tag{20}$$

Other physical and transport properties can be determined when $T_{wet,m}^{j+1}$ is found.

The airflow model has two non-linear, governing partial differential equations. At the time step $(j+1)$, the discretized forms for Eqs. (12) and (13) may be expressed using the implicit forward-difference approximation [28]

$$\rho_{a^\infty}\Delta z\frac{Y_m^{j+1}-Y_m^{j}}{\Delta t}+j_{a^\infty}\frac{Y_{m+1}^{j+1}-Y_m^{j+1}}{\Delta z}\Delta z=\dot{m}_m^{j+1}, \tag{21}$$

$$\begin{aligned}&(c_{pa}+Y_m^jc_{pv})\\&\quad\times\left(\rho_{a^\infty}\Delta z\frac{T_{a^\infty,m}^{j+1}-T_{a^\infty,m}^{j}}{\Delta t}+j_{a^\infty}\frac{T_{a^\infty,m+1}^{j+1}-T_{a^\infty,m}^{j+1}}{\Delta z}\Delta z\right)\\&\quad=q_{tot,m}^{j+1}.\end{aligned} \tag{22}$$

Rearranging Eqs. (21) and (22) and recognizing that $j_{a^\infty}=\rho_{a^\infty}(\Delta z/\Delta t)$, the discretized humidity ratio and air temperature at the time step $(j+1)$ and the space step $(m+1)$, respectively, are

$$Y_{m+1}^{j+1}=Y_m^j+\frac{\dot{m}_m^{j+1}}{j_{a^\infty}} \tag{23}$$

$$T_{a^\infty,m+1}^{j+1}=T_{a^\infty,m}^{j}+\frac{q_{tot,m}^{j+1}}{j_{a^\infty}(c_{pa}+Y_m^jc_{pv})} \tag{24}$$

The implicit finite difference method, which is known to yield stable solutions for any selection of the space and time nodal points, is used to solve the yarn and airflow models. Since the dependent variables in the two models are interrelated, the two models must be solved simultaneously. Based on the numerical methods discussed above, the algorithm to solve the transient through-air drying model is illustrated in Fig. 5.

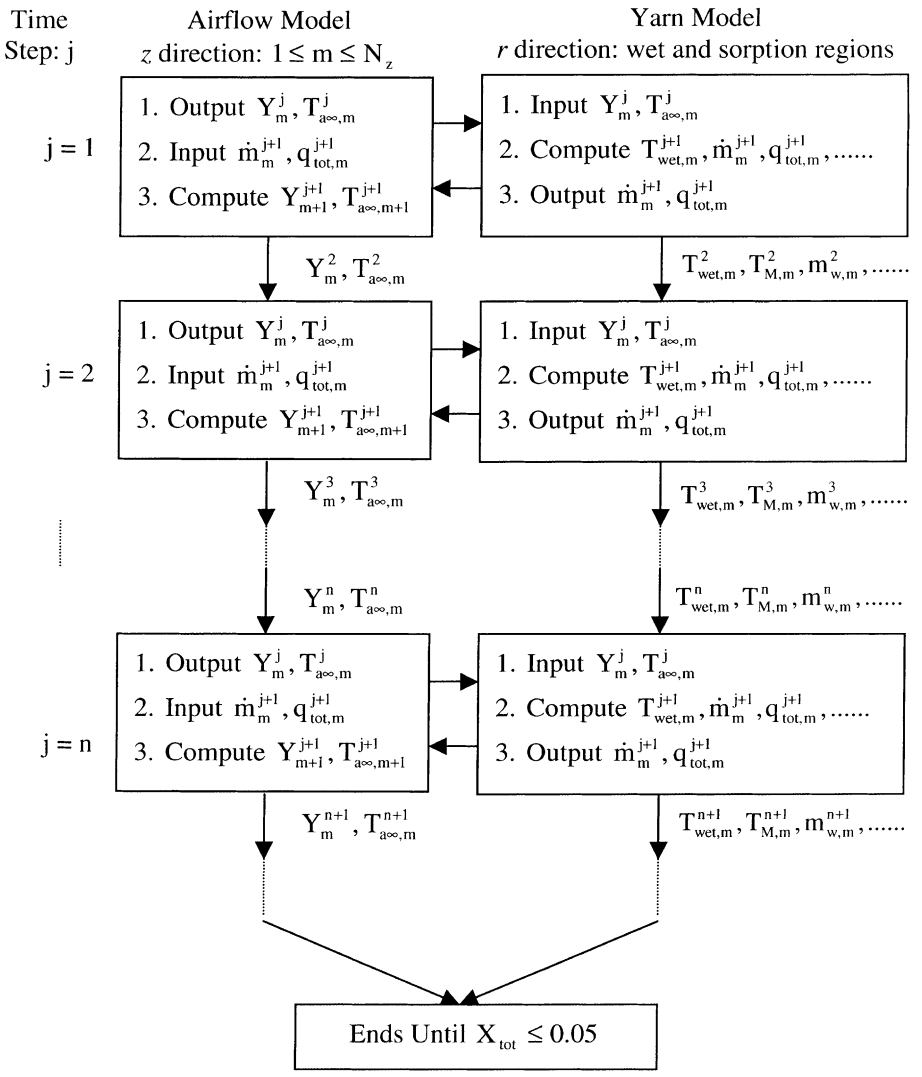

Fig. 5. Algorithm for solving the coupled models.

At the time step (j), the values of $\dot{m}_m^{j+1}$ and $q_{\mathrm{tot},m}^{j+1}$ obtained in the yarn model are substituted into the airflow model to get the values of Y_{m+1}^{j+1} and $T_{a^\infty,m+1}^{j+1}$ for a space step (m). The values of Y_{m+1}^{j+1} and $T_{a^\infty,m+1}^{j+1}$ are then substituted into the yarn model for the space step $(m+1)$ at the next time step. To control the values of Y_{m+1}^{j+1} and $T_{a^\infty,m+1}^{j+1}$ used in computing for the space step $(m+1)$ at the next time step, the following numerical criterion is used:

$$\Delta t = \frac{\varepsilon_c}{V_{a^\infty}} \Delta z. \tag{25}$$

This relationship was obtained by setting the computational time step equal to the time required for air to travel a differential length (Δz) in the pile yarn direction.

All the physical and transport properties can be determined from correlations in the literature [12] except the three unknown transport properties, D_{eff}, h_T and h_m. They must be determined by the best fit to the experimental data.

At the time step (j), effective diffusivity ($D_{\mathrm{eff},m}^j$) is expressed as

$$D_{\mathrm{eff},m}^j = \left\{ 2.23 \times 10^{-5} \left[\frac{0.5(T_{\mathrm{surf},m}^j + T_{\mathrm{wet},m}^j)}{273.15} \right]^{1.75} \right\} \Big/ \tau. \tag{26}$$

Thus, the value of the correction factor, τ, is determined by the best fit to the experimental data. At the time step (j), the heat transfer coefficient is expressed as

$$h_{T,m}^{j} = h_{T0}\left[0.5 + 0.5\frac{X_m^j}{X_{\text{crit}}}\right]. \quad (27)$$

Once the value of h_{T0} is determined by the best fit to the experimental data, the mass transfer coefficient may be determined by the following equation [29]:

$$\frac{h_{T0}}{h_{m0}} = \rho c_{\text{p}} Le^{0.667}, \quad (28)$$

where ρ is the density of the air, c_{p} is the specific heat capacity of the air and Le is the dimensionless Lewis number. Therefore, there are only two parameters to be determined by the best fit to the experimental data.

4. Experimental program

4.1. Magnetic resonance imaging (MRI) system

A Bruker DSX-400 magnetic resonance imaging (MRI) scanner, operating at a ^{1}H frequency of 400 MHz (9.4-T magnet), is used to continuously record one-dimensional projections of the moisture in a wet carpet sample positioned in an imaging probehead. Experimental details for quantitative imaging of moisture profiles in carpet are described elsewhere [25,30]. A one-dimensional single-point imaging sequence was used here with a 1.3-μs excitation pulse, a 40-μs detection delay, and a 50-ms repetition time. Two-dimensional (2D) images of moisture in a single carpet yarn were measured with a FLASH imaging sequence using 1.9-ms echo times and 50-ms repetition delays. Each 2D image was recorded in about 15 s [31].

As shown in Fig. 6, the imaging probehead, placed directly inside the magnetic field, contains a sample holder whose outer diameter is 25 mm. The sample holder is composed of two open-ended glass tubes that hold the carpet sample in place and direct the airflow entirely through the sample. The sample is surrounded by a radio frequency coil that serves as both transmitter and receiver coil for MRI. Details of the sample holder and MRI probehead assembly are provided elsewhere [12,24]. Airflow rate and air temperature are controlled by the Bruker system. Airflow rate is measured using an OMEGA FMA1826 flowmeter. Air temperature is measured by a thermocouple positioned in front of the carpet sample and used to control a resistance heater located upstream from the sample.

4.2. Laboratory through-air dryer (LTAD)

Drying tests were also conducted using a LTAD. The LTAD was designed and built to simulate the drying process occurring in industrial through-air dryers. In the blower and control section, air is drawn in by a blower driven by a 5-hp motor, and the airflow rate is controlled

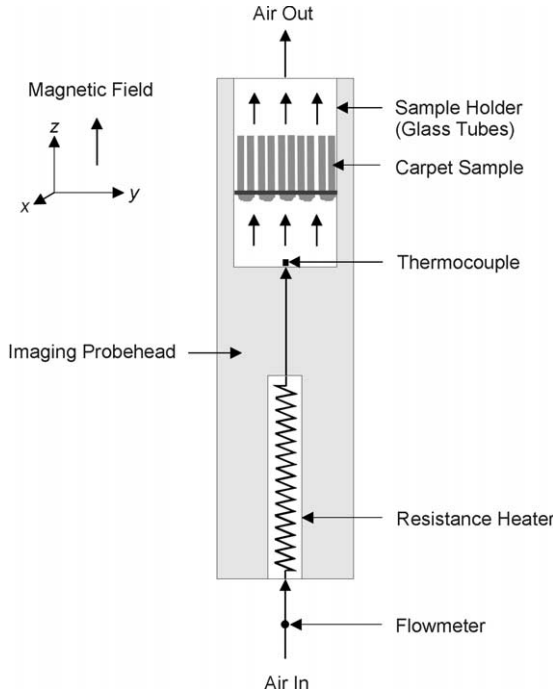

Fig. 6. Schematic of the MRI probehead assembly used for through-air drying studies.

by an adjustable damper. As the air comes into the temperature and humidity control section, it is heated principally by electrical coils and secondarily by steam coils. Temperature is controlled using an OMEGA CN4400 temperature controller.

Several variables are measured in the test section. They are the upstream and downstream dry bulb temperatures and relative humidities of the moist air, the apparent velocity of air passing through the sample, the average pressure drop across the sample, the temperature of the sample, and the weight of the sample during the drying process. At the data acquisition computer section, data are collected by a PC 486DX66 via Labtech Notebookpro version 10 software via RS232 communicative or analog output signals.

4.3. Materials, samples preparation and procedure

Two commercial unbacked cut-pile nylon greige carpet samples A and B were used in the through-air drying tests for which numerical solutions were obtained. Carpet construction parameters of the samples are given in Table 1.

The samples used in the MRI probehead were 18 mm in diameter, and the samples used in the LTAD were 30.5 cm in diameter. Before through-air drying, the moisture regain in carpet is typically lowered through vacuuming. In our tests, a laboratory vacuuming system

Table 1
Values of the carpet construction parameters for carpet samples A and B

Parameters	Sample A	Sample B
R (mm)	1.5	2.0
L (mm)	19.0	11.7
m_y (g)	9.95×10^{-3}	6.53×10^{-3}
ε_c	0.62	0.45
ε_y	0.75	0.85

was used to reduce the overall moisture regain to approximately 50%. The MRI study revealed that vacuuming procedures affected the initial moisture profiles [12]. Details of sample preparation and procedure are given in reference [12].

5. Results and discussions

Numerical solutions for several cases were obtained using the numerical method described above. Local and overall moisture regains were predicted as a function of drying time for two types of carpet, two airflow rates, two air temperatures, two airflow directions and three initial moisture profiles. The initial moisture profiles measured by MRI were used as initial conditions for the numerical simulations. The values of two transport parameters, τ and h_T, were adjusted for best fit to the MRI experimental data, and h_m was calculated using Eq. (28). Table 2 gives the values of the transport parameters for several drying conditions.

5.1. Comparison of numerical results with MRI results

The predicted local and overall moisture regains versus time agreed very well with the experimental data for all cases simulated. Representative examples are shown in Figs. 7 and 8 where the predicted and experimental results are plotted for carpet samples A and B. For these tests, the airflow, which enters the carpet face, is at an air temperature of 80°C and an airflow rate of 20 m/min. The initial overall moisture regain for the two carpets is 50%, but the initial moisture distributions are different. As illustrated in Figs. 7 and 8, the predicted moisture profiles agree well with experimental data. Additionally, the predicted overall moisture regain versus drying time fits the experimental data very well as illustrated in Fig. 9.

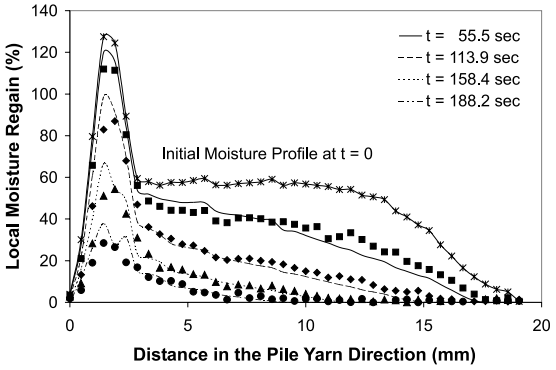

Fig. 7. Comparison of MRI experimental and predicted moisture distribution versus time for carpet sample A at an airflow rate of 20 m/min and an air temperature of 80°C. Numerical fits to the data are shown as lines.

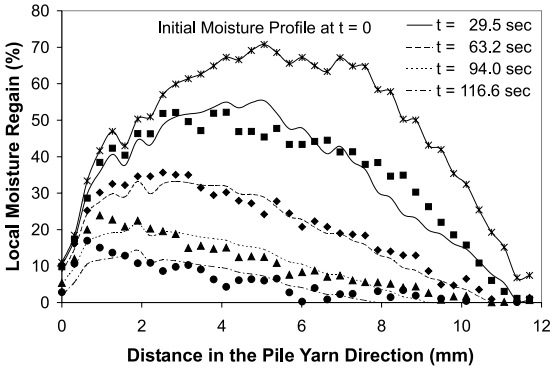

Fig. 8. Comparison of MRI experimental and predicted moisture distribution versus time for carpet sample B at an airflow rate of 20 m/min and an air temperature of 80°C. Numerical fits to the data are shown as lines.

Table 2
Values of the transport parameters at different drying conditions for carpet samples A and B

Parameter	Sample A				Sample B			
$V_{a\infty}$ (m/min)	20	20	30	30	20	20	30	30
$T_{a\infty 0}$ (°C)	353	389	353	389	353	389	353	389
Y_0 (kg_w/kg_a)	0.0029	0.088	0.0029	0.088	0.0029	0.088	0.0029	0.088
τ	16.7	16.7	16.7	16.7	13.7	13.7	13.7	13.7
h_{T0} (W/m^2 K)	56.0	56.0	68.6	68.6	66.1	66.1	80.9	80.9
h_{m0} (m/s)	0.056	0.072	0.068	0.089	0.066	0.085	0.080	0.105

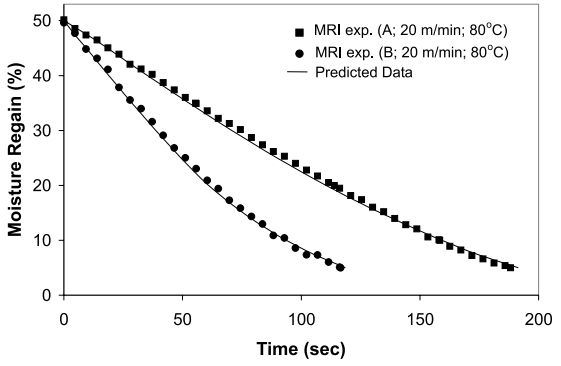

Fig. 9. Comparison of MRI experimental and predicted overall moisture regain versus time for carpet samples A and B at an airflow rate of 20 m/min and an air temperature of 80°C. Overall moisture regain data were obtained by integrating the moisture profiles.

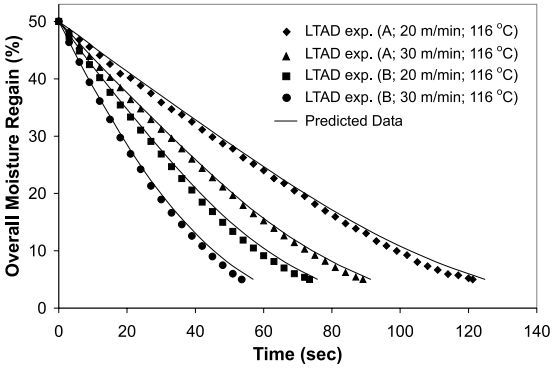

Fig. 10. Comparison of LTAD experimental and predicted variations of overall moisture regain with time for carpet samples A and B at airflow rates of 20 and 30 m/min, and an air temperature of 116°C.

5.2. Comparison of numerical results with LTAD results

The simplified mathematical model was verified by the MRI drying results, however, the air temperature used in the MRI system (80°C) is less than that used in the first few zones of industrial dryers (typically >110°C). Thus, the LTAD drying results were used to verify the model at industrial drying conditions.

Since the LTAD cannot measure the local moisture distribution, the verification focused on predicting the variations of overall moisture regain (average for entire sample) with drying time. The initial moisture distribution was assumed to be uniform because initial moisture distribution does not greatly affect the overall drying results [12]. For the numerical simulations, the same carpet construction parameters used for drying at 80°C in the MRI scanner were used for simulating the LTAD tests performed at an air temperature of 116°C. The numerical results for the LTAD tests were obtained using the heat transfer coefficient and correction factor found in the 80°C MRI tests and the mass transfer coefficient calculated using Eq. (28). For drying carpet samples A and B at airflow rates of 20 and 30 m/min, the predicted and experimental variations of overall moisture regain are plotted in Fig. 10. As shown in this figure, the predicted drying curves fit the experimental data quite well.

Several drying tests were conducted at different airflow rates, air temperatures, airflow directions and initial moisture profiles and compared with the numerical predictions. Close agreements with the experimental MRI and LTAD results were obtained [12]. Thus, the simplified mathematical model can accurately predict drying rate and drying time for through-air drying of tufted carpet.

6. Conclusions

A transient two-dimensional mathematical model has been developed to simulate the through-air drying process for tufted textile materials. Even after simplifying the model to facilitate its usability, it provides predictions that closely agree with experimental results. Predicted variations of one-dimensional moisture distributions within carpet agree well with profiles obtained using MRI. Predicted temporal variations of overall moisture regain closely fit experimental results obtained with both MRI and the LTAD.

Acknowledgements

This work was supported by the National Textile Center. We are grateful to Dr. Morton Reed of Milliken Carpet and Mr. David Wright of Queen Carpet Corp. for many helpful discussions and for providing samples.

References

[1] Carpets and Rugs, Industrial Brief, vol. 1(15R), Electric Power Research Institute, Palo Alto, CA, 1995.
[2] J.D. Brock, C.W. Gorton, Through-flow drying of tufted textile materials, Text. Res. J. 34 (12) (1964) 1031–1039.
[3] G. Arnaud, J.-P. Fohr, Slow drying simulation in thick layers of granular products, Int. J. Heat Mass Transfer 31 (12) (1988) 2517–2526.
[4] P. Chen, D.C.T. Pei, A mathematical model of drying processes, Int. J. Heat Mass Transfer 32 (2) (1989) 297–310.
[5] P. Chen, P.S. Schmidt, An integral model for drying of hygroscopic and non-hygroscopic materials with dielectric heating, Drying Technol. 8 (5) (1990) 907–930.

[6] P. Chen, P.S. Schmidt, A model for drying of flow-through beds of granular products with dielectric heating, in: Transport Phenomena in Materials Processing – 1990, American Society of Mechanical Engineers, Heat Transfer Division, (Publication) HTD, vol. 146, ASME, New York, 1990, pp. 121–127.
[7] C. Dietl, O.P. George, N.K. Bansal, Modeling of diffusion in capillary porous materials during the drying process, Drying Technol. 13 (1&2) (1995) 267–293.
[8] N.D. Francis, W.J. Wepfer, Jet impingement drying of a moist porous solid, Int. J. Heat Mass Transfer 39 (9) (1996) 1911–1923.
[9] G.R. Hadley, Numerical modeling of the drying of porous materials, in: Proceedings of the Fourth International Drying Symposium, vol. 1, 1984, pp. 151–158.
[10] J.G. Hartley, Coupled heat and moisture transfer in soils: a review, Adv. Drying 4 (1987) 199–248.
[11] M. Ilic, I.W. Turner, Convective drying of a consolidated slab of wet porous material, Int. J. Heat Mass Transfer 32 (12) (1989) 2351–2362.
[12] H.S. Lee, Study of the industrial through-air drying process for tufted carpet, Ph.D. Thesis, Georgia Institute of Technology, Atlanta, GA, 2000.
[13] A.V. Luikov, Heat and Mass Transfer in Capillary-Porous Bodies, Pergamon Press, Oxford, 1966.
[14] A.V. Luikov, Systems of differential equations of heat and mass transfer in capillary-porous bodies, Int. J. Heat Mass Transfer 18 (1975) 1–14.
[15] S.B. Nasrallah, P. Perre, Detailed study of a model of heat and mass transfer during convective drying of porous media, Int. J. Heat Mass Transfer 31 (5) (1988) 957–967.
[16] M.A. Stanish, G.S. Schajer, F. Kayihan, A mathematical model of drying for hygroscopic porous media, AIChE J. 32 (8) (1986) 1301–1311.
[17] R. Toei, Drying mechanism of capillary porous bodies, Adv. Drying 2 (1983) 269–297.
[18] S. Whitaker, Simultaneous heat, mass, and momentum transfer in porous media: A theory of drying, in: J.P. Harnett, T.F. Irvine (Eds.), Advances in Heat Transfer, vol. 13, Academic Press, New York, 1977, pp. 119–203.
[19] S. Whitaker, Heat and mass transfer in granular porous media, in: A.S. Mujumdar (Ed.), Advances in Drying, vol. 1, Hemisphere, New York, 1980, pp. 23–61.
[20] S. Whitaker, W.T.-H. Chou, Drying granular porous media theory and experiment, Drying Technol. 1 (1) (1983) 3–33.
[21] S. Whitaker, Moisture transport mechanisms during the drying of granular porous media, in: Drying '85, Hemisphere, New York, 1985, pp. 21–32.
[22] K.M. Waananen, J.B. Litchfield, M.R. Okos, Classification of drying models for porous solids, Drying Technol. 11 (1) (1993) 1–40.
[23] W.W. Carr, H.W. Beckham, H.W. Spiess, C. Fulber, B. Blümich, Nuclear-magnetic-resonance imaging of water distributions in loop-pile nylon carpet tiles, J. Text. Inst. 89 (2) (1996) 436–440.
[24] J. Leisen, L. Hou, H.W. Beckham, W.W. Carr, Observation of the water distribution during drying of textiles, in: Spatially Resolved Magnetic Resonance, Wiley, New York, 1998, pp. 265–272.
[25] J. Leisen, H.W. Beckham, Experimental considerations for the application of magnetic resonance imaging in the textile sciences, Text. Res. J. (in press).
[26] H.S. Lee, W.W. Carr, H.W. Beckham, W.J. Wepfer, Factors influencing air flow through unbacked tufted carpets, Text. Res. J. 70 (10) (2000) 876–885.
[27] W.Z. Black, J.G. Hartley, Thermodynamics, Harper & Row, New York, 1985.
[28] C.F. Gerald, P.O. Wheatley, Applied Numerical Analysis, fourth ed., Addison-Wesley, Reading, MA, 1989.
[29] F.P. Incropera, D.P. DeWitt, Fundamentals of Heat and Mass Transfer, second ed., Wiley, New York, 1985.
[30] S. Gravina, D.G. Cory, Sensitivity and resolution of constant-time imaging, J. Magn. Reson., Ser. B 104 (1994) 53–61.
[31] P.T. Callaghan, Principles of Nuclear Magnetic Resonance Microscopy, Clarendon Press, Oxford, 1991.